Journal of Human Centered Technology

https://www.humentech.utm.my E-ISSN: 2821-3467

Physicochemical and Thermal Analysis of Silane-Modified Carbonated Hydroxyapatite Fillers for Periodontal Application

Reza Pahlevi Rudianto[1,2], Dida Faadihilah Khrisna[1], Yogi Angga Swasono[3], Bidhari Pidhatika[4,5], Syafiqah Saidin[1,6]*

[1]Department of Biomedical Engineering and Health Sciences, Faculty of Electrical Engineering, Universiti Teknologi Malaysia, 81310 UTM Johor Bahru, Johor, Malaysia
[2]Research Center for Polymer Technology, National Research and Innovation Agency (BRIN), Banten 15343, Indonesia
[3]Research Center for Food Technology and Processing, National Research and Innovation Agency (BRIN), Gading, Playen, Gunungkidul, Yogyakarta, 55861, Indonesia
[4]Polytechnic Institute of Nuclear Technology, National Research and Innovation Agency (BRIN) Indonesia, Yogyakarta 55281, Indonesia
[5]Research Collaboration Center for Biomedical Scaffolds, National Research and Innovation Agency of the Republic of Indonesia and Universitas Gadjah Mada, Sekip Utara, Yogyakarta 55283, Indonesia
[6]IJN-UTM Cardiovascular Engineering Centre, Institute of Human Centered Engineering, Universiti Teknologi Malaysia, 81310 UTM Johor Bahru, Johor, Malaysia

*Corresponding Author syafiqahsaidin@biomedical.utm.my

Cite: https://doi.org/10.11113/humentech.v5n2.148 Research Article

Abstract:
Periodontal disease is a chronic inflammation affecting the teeth's supporting structures that, if untreated, can lead to tooth loss. To address this issue, biomaterial-based approaches are currently being explored, requiring materials that are biocompatible and capable of supporting bone regeneration. Carbonated hydroxyapatite (CHA) has shown promise for periodontal applications due to its biocompatibility and enhanced bioactivity compared to stoichiometric hydroxyapatite. However, surface modification of CHA is necessary to improve its performance as a filler in composite biomaterials. To address this, two silane coupling agents, tetraethyl orthosilicate (TEOS) and 3-(trimethoxysilyl)propyl methacrylate (TMSPMA) were evaluated at different reaction temperatures. Physicochemical and thermal analyses were conducted to determine the optimal strategy for modifying the CHA surface. The physicochemical analyses confirmed successful carbonation and silanization of CHA, with higher reaction temperatures yielding more extensive and homogeneous silane condensation on the surface. The elemental analysis revealed that the CHA modified with TEOS at 78.3°C possessed the highest silicon content among all groups. Furthermore, silanization process enhanced the thermal stability of CHA. Thus, silanization at elevated temperatures has effectively modified the CHA matrix, with TEOS modification at 78.3°C identified as the optimal strategy for periodontal biomaterial applications.

Keywords: Periodontal disease; Carbonated hydroxyapatite; Silanization

1. INTRODUCTION

Periodontal disease is a common chronic inflammatory condition that is progressively affected by a destructive process of supporting tissues of the teeth, including the periodontal ligament, cementum, and alveolar bone, which may eventually result in tooth loss if left untreated (1–3). Current treatments for periodontal disease can stop the progression of the disease and establish healthy gingiva, but they are incapable of inducing and regenerating the lost tissues (4–6). There is a constant demand for biomaterials that can stimulate new bone formation and therefore can aid in the regeneration of lost periodontal tissues. These biomaterials for periodontal bone replacement should be biocompatible (7–9) and release at a controlled rate (10) to support new bone formation. The biomaterial should also be able to provide adequate mechanical support to allow healing of the newly formed bone (11).

Among synthetic calcium phosphate biomaterials, hydroxyapatite (HA) is one of the most studied due to its chemical similarity with the bone mineral phase and its established biocompatibility (12,13). However, stoichiometric HA presents low solubility and slow resorption, thereby limiting its compatibility with the natural process of bone remodeling (14). Ionic substitution and functionalization to improve the bioactivity of HA have been studied in previous research. For fluorapatite, fluoride ions are designed to replace hydroxyl groups where this material has enhanced the material's chemical stability and resistance to acidic environments (15). Magnesium-substituted HA has demonstrated significant potential to enhance osteogenic cell attachment and bioactivity (16,17). Despite these advances, achieving a refined balance between rapid degradation and mechanical integrity to stabilize periodontal defect remains a critical challenge in current clinical applications (18). The presence of carbonate ions in the bone mineral has triggered special interest in the development of carbonated hydroxyapatite (CHA) (19). Carbonated hydroxyapatite presents higher bioactivity (20), solubility (21), and

Received 29 July 2026; Accepted 03 August 2026
Available online 06 August 2026

biodegradability (22) than stoichiometric HA, allowing it to resorb gradually while creating a favorable environment for new bone growth (23). However, surface modification of CHA to improve its performance as a filler in composite biomaterials is challenging due to the hydrophilic surface, which tends to form agglomerates through chemical interactions between its hydroxyl groups.

Previously, the surface of bio-ceramics has been modified by silane coupling agents. The physicochemical properties of the bio-ceramics have been improved to be well dispersed in polymeric matrices (24), have interfacial adhesion (25), and better thermal stability (26). There have been reports on the surface modification of bio-ceramics with functional organosilanes such as methacrylate-containing silane (27), non-methacrylate silane (28), and inorganic silica precursors (29). However, most of the reports are limited to the surface modification of conventional HA with a single type of silane coupling agent under fixed processing conditions. For CHA, there have been only a few reports on the surface modification with different types of silane precursors (30) and the influence of reaction temperature (31) on the surface modification. Thus, how silane precursor types across various reaction temperatures affect the physicochemical and thermal properties of modified CHA needs to be thoroughly investigated. In this study, CHA was prepared from HA and modified with silane coupling agents of different chemical structures at various temperature processes. The physicochemical and thermal properties of modified CHA were evaluated, and the results were discussed in terms of surface modification. The findings of this study will be useful to select an appropriate surface modification method for the preparation of advanced CHA-based periodontal fillers.

2. MATERIALS AND METHODOLOGY

2.1 Materials Preparation

Chemicals used in this study, namely hydroxyapatite, sodium carbonate, ammonium hydroxide, ethanol, acetic acid, tetraethyl orthosilicate (TEOS) and 3-(trimethoxysilyl)propyl methacrylate (TMSPMA) were purchased from Sigma-Aldrich (USA), while nitric acid was sourced from SMART-LAB (Indonesia). Carbonated hydroxyapatite was prepared through a wet chemical precipitation method (32) in which 5 g of HA was suspended in 100 mL of deionized water and stirred for 1 h. The dissolution process was then carried out by adding 2 M nitric acid dropwise and stirring for 1 h at room temperature until a transparent solution with pH of less than 3 was formed. In a separate beaker, 0.5 g of sodium carbonate was dissolved in 20 mL of DI water and then added dropwise to the transparent HA solution and stirred continuously for 30 min. The pH of the mixture was then adjusted and maintained at 10 by gradual addition of ammonium hydroxide. The resulting suspension was centrifuged at 5000 rpm for 5 min to collect the precipitate. The precipitate was then dried in an oven at 80°C for 24 h and labelled as CHA.

The silanization process, shown in Figure 1, was conducted by dispersing 1.3 g of CHA in 26 mL of ethanol and stirring for 15 min at room temperature. Then, 0.4 mL of acetic acid was added, and the mixture was stirred for an additional 30 min at room temperature. The modification was performed by adding 0.13 mL of silane precursor and stirring for 1 h while maintaining the process temperature at either room temperature or 78.3°C. Two different silane precursors, inorganic (TEOS) and organic (TMSPMA), were used in this study to examine the effect of different silanes on the CHA. Precipitates were then isolated from the suspension by centrifugation at 5000 rpm for 5 min and washed with ethanol (3 times) using vortex mixing. The resulting material was dried in an oven at 80°C for 24 h. In total, four different samples were examined in this study, as detailed in Table 1.

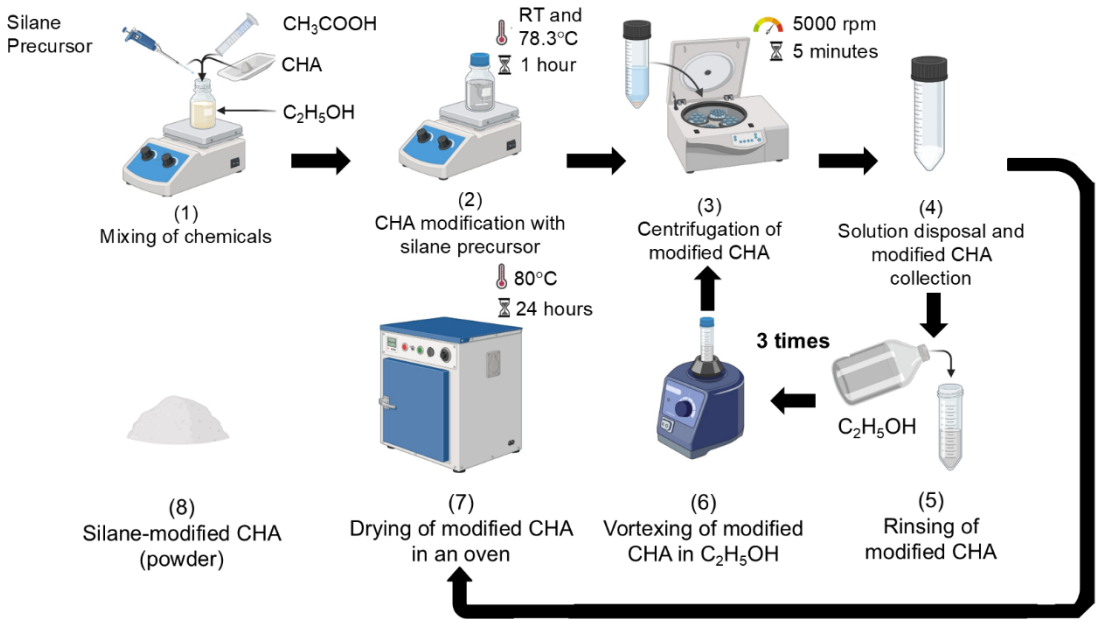

Figure 1. Silanization process of CHA that included solution mixture preparation (step 1), CHA modification (step 2), and washing and collection of modified CHA (step 3 to 8). Figure 1 was created using Biorender.

Table 1. List of sample codes determining the prepared samples.

Sample Code	Sample
CT1	CHA modified with TEOS at room temperature
CT2	CHA modified with TMSPMA at room temperature
CM1	CHA modified with TEOS at 78.3°C
CM2	CHA modified with TMSPMA at 78.3°C

2.2 Characterization

The silane-modified CHA, namely CT1, CT2, CM1, and CM2 (as detailed in Table 1) were analyzed using a Fourier Transform Infrared (FTIR) spectrometer equipped with an attenuated total reflectance (ATR) accessory (Alpha II, Bruker, US) at a wavenumber range of 400–4500 cm^{-1}. Visualization and elemental composition analysis of the silane-modified CHA was done using scanning electron microscopy-energy dispersive X-ray (SEM-EDS, JEOL 6150LA, JP) at a magnification of 500×. The samples were also subjected to X-ray diffraction (XRD) analysis (Aeris, Malvern Panalytical, UK) to analyze the crystallinity of the materials. Thermogravimetric analysis (TGA), an analytical technique that combines gravimetric and thermal analysis to characterize the thermal properties of a material, was conducted using a TGA instrument (STA 6000, Perkin Elmer, US) to investigate physical and chemical changes, such as dehydration, decomposition, and degradation, in the material. The samples were heated at a rate of 10°C/min under an inert atmosphere (N_2). The temperature range of the thermal analysis was set at 50–800°C.

3. RESULTS AND DISCUSSION

3.1 FTIR Analysis

The FTIR spectra of HA and CHA from the carbonation process were analyzed to verify the functional groups. The FTIR spectra in Figure 2 (a) (blue line) indicated the presence of several functional groups, namely phosphate (PO_4^{3-}), hydroxyl (O–H), and adsorbed water groups, which belong to the HA (33). Strong peaks at 564 and 1067 cm^{-1} indicated the existence of phosphate groups (34). This is followed by strong peaks at 3450 and 3571 cm^{-1}, which are the characteristic of O–H stretching (35). Figure 2 (a) (red line) of the FTIR spectra reveals several functional groups of HA, including the emergence of a new functional group at 3142 cm^{-1} (shoulder bond) and an increased intensity of the carbonate group at 1386 cm^{-1} (36). Furthermore, the decrease in intensity of the phosphate group at 1067 and 564 cm^{-1} suggests an ion exchange process between PO_4^{3-} and CO_3^{2-} ions during the carbonation of HA, resulting in the formation of type B HA (37).

The FTIR spectra of the silane-modified CHA samples produced through various silanization processes, shown in Figure 2 (b) indicates the presence of functional groups characteristic of CHA. The appearance of new functional groups at 1064 and 860 cm^{-1} suggests the formation of silanol and organosilane groups (38). Among all sample variations, sample CM1 exhibited the highest peak intensity for nearly every functional group. This implies that the synthesis conditions for sample CM1 were optimal and could be replicated to produce silane-modified CHA for subsequent fabrication of GTR membranes.

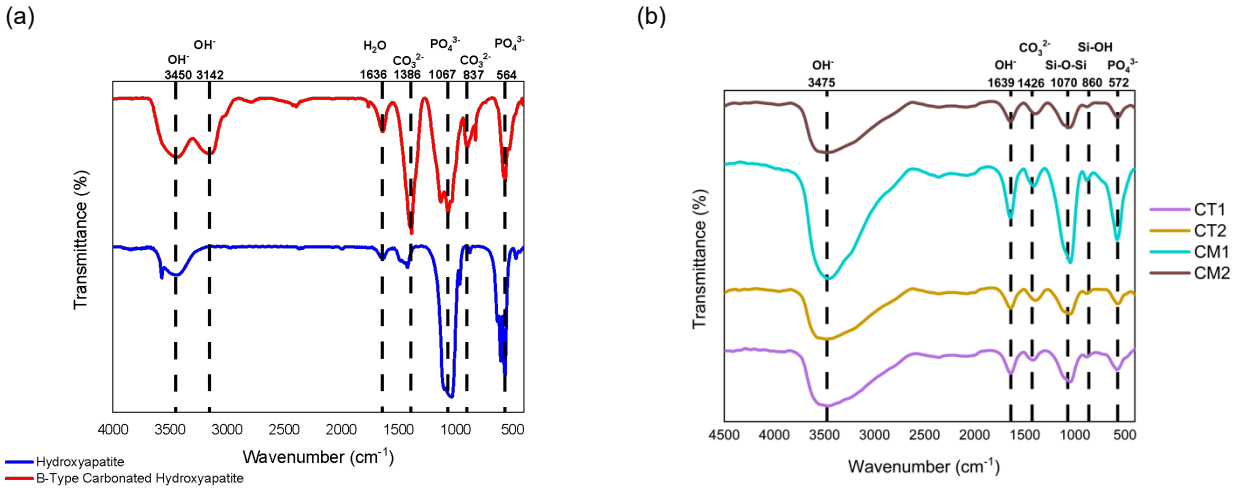

Figure 2. FTIR spectra of (a) HA and CHA, and (b) silane-modified CHA processed using various temperatures and silane precursors (as detailed in Table 1).

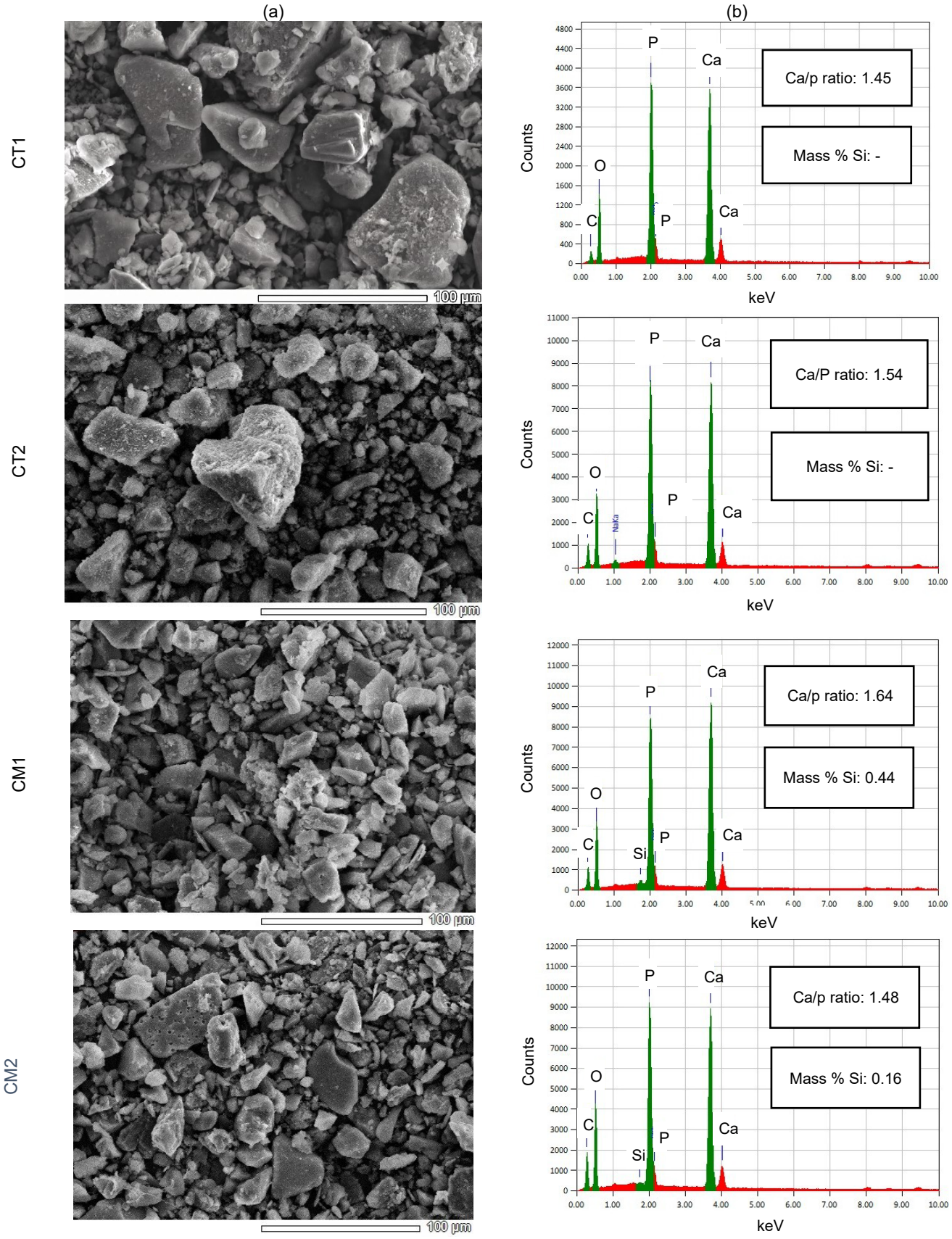

Figure 3. (a) SEM images and (b) corresponding EDS spectra of silane-modified CHA (CT1, CT2, CM1, and CM2) with variations detailed in Table 1.

3.2 Elemental Analysis

Figure 3 presents the SEM micrographs and the corresponding EDS spectra of the silane-modified CHA. The SEM images revealed a change in morphology in silanized CHA with increasing reaction temperature. The samples prepared at room temperature exhibited a more heterogenous particle size distribution, with coarser, irregularly shaped agglomerates with finer fragments scattered throughout. In contrast, the samples treated at 78.3°C exhibited finer, more uniform granular morphology with closer particle packing, suggesting that the elevated temperature promoted more extensive and homogeneous silane condensation on the CHA surfaces. The CM showed the most pronounced response, reaching the highest mass of Si without showing any significant change in the calcium-to-phosphate ratio. This observation is consistent with the known thermal activation of alkoxysilane polymerization, where elevated reaction temperatures accelerate silanol-to-siloxane condensation kinetics, promoting covalent chemisorption over loose physical adsorption (39).

Furthermore, the content of Si in the surface of CM1 was found to be 0.44%, whereas that of CM2 was 0.16%. These results indicate that TEOS as an inorganic silane precursor is more efficient for the introduction of silicon into the material than TMSPMA as an organic silane precursor. The TEOS underwent hydrolysis and condensation reactions to form silanol species, which were dissolved in the solution and penetrated into the pores of CHA and filled up the spaces between them (40). Silanol and organosilane species also reacted with the surface groups of the material to form a surface layer of CHA (41). In contrast, TMSPMA contains bulky trimethylsilyl functional groups alongside hydrolysable alkoxy groups (42). It is an organic silane coupling agent, containing an organofunctional methacrylate group (43). The lower content of Si in the TMSPMA-modified CHA can be due to limited extent of condensation reactions of the silane groups, possible loss of organic part of the modifier during the processing, and/or the formation of a very thin surface coupling layer (44).

3.3 XRD Analysis

Figure 4 (a) and (b) show the XRD patterns for HA and silanized CHA, respectively. All four silanized samples retained the characteristic diffraction peaks of HA, notably the prominent (002) reflection near 26° and the unresolved triplet cluster in 31–34° region (211, 112 and 300 planes), alongside weaker secondary reflections near 40°, 47°, 50° and 53°. This confirms that the underlying apatite crystal structure survived both carbonation and silanization, which aligns with the retention of phosphate and hydroxyl functional groups identified through the FTIR in Figure 2 (a).

Compared to the pure HA, the silane-modified CHA samples displayed peak broadening and a higher, less-defined baseline, pointing to reduced crystallinity. This decrease was attributed to the incorporation of CO_3^{2-} ions into the apatite lattice, which is known to introduce lattice strain and disrupt long-range crystalline order, consistent with the carbonate-associated bands identified in the FTIR spectra from Figure 2 (a) and the proposed PO_4^{3-}/CO_3^{2-} ion-exchange mechanism (45,46). This is also in line with a study by Cisneros-Pineda et al. (47), which found that silanized HA was reduced in its crystallinity due to the presence of silane agent. The broad background signal across 20–35° likely reflected a minor contribution from amorphous silica or siloxane species formed during the silanization (47,41), further supported by the Si–O–Si and Si–OH FTIR bands observed in all four samples.

Among the four silanized samples, CM1 and CM2 exhibited sharper and more intense diffraction peaks at 26° and within the 31–34° cluster compared to CT1 and CT2. This indicates higher retained crystallinity when silanizing at 78.3°C compared to room temperature. Due to no peak shifts was detected across any sample, the silanization appeared to alter peak intensity and width rather than unit cell dimensions (32). This trend is consistent with the SEM-EDS results, in which the samples treated at 78.3°C showed measurable silicon content, whereas no silicon was detected at room temperature, suggesting that a more complete and uniform silane surface coating at elevated temperature may help preserve crystalline order relative to the less extensive coating formed at room temperature (39).

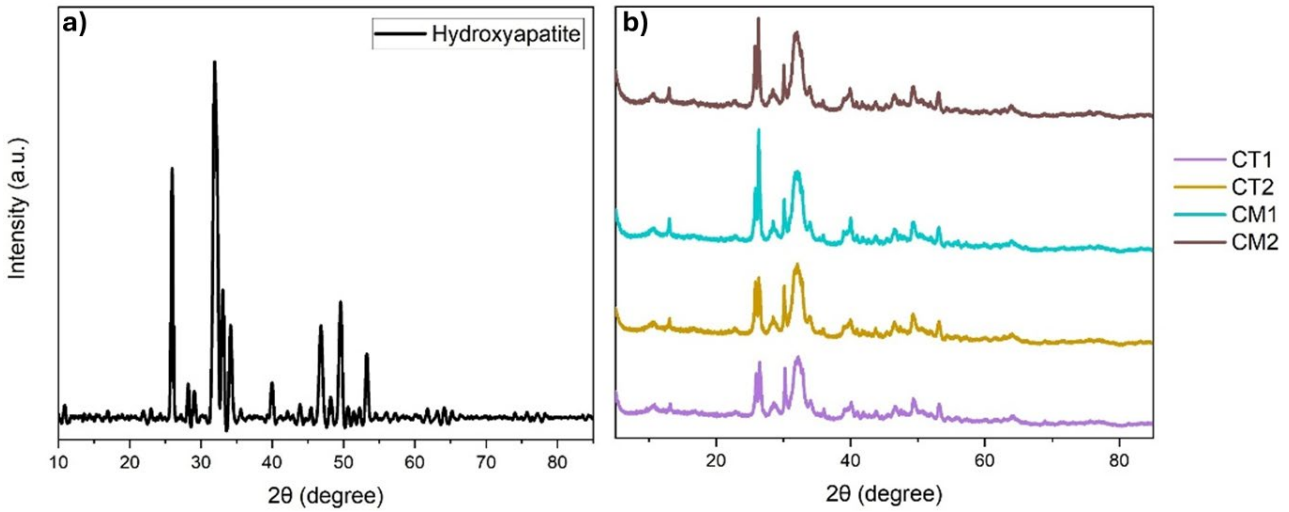

Figure 4. XRD spectra of (a) HA and (b) silane-functionalized CHA with variations detailed in Table 1.

3.4 Thermal Analysis

The thermal analysis results for CHA and silane-modified CHA processed at higher temperature, specifically CM1 and CM2, are presented in Figure 5. The thermogravimetric (TG) plots of percent weight against temperature reveal distinct degradation patterns influenced by the presence and type of silane precursor. The samples generally exhibited a three-step degradation process. The initial step, occurring around 200°C, was attributed to the dehydration and removal of adsorbed water. The maximum weight loss of 5.86% was observed for the pure CHA, while the minimum loss of 1.29% was recorded for the TEOS-modified CHA (CM1). These data suggest, the removal of absorbed moisture from the sample surface was more significant in the pure CHA (48).

In the second step, occurring at 200–500°C, similar weight loss was observed between CM1 and CM2. In contrast, the pure CHA experienced a significant weight loss of 19.87%, primarily due to the loss of structural water around 280°C and subsequent reaction between two molecules of calcium monohydrogen phosphate and water around 450°C (49). The third step represents a relatively stable step in the thermal analysis, corresponding to the decarboxylation and dihydroxylation of CHA (49). The total weight losses for CHA (non-modified), TEOS-modified CHA (CM1), and TMSPMA-modified CHA (CM2) were 27.36%, 10.04%, and 9.88%, respectively. The reduced weight loss observed in CM1 and CM2 indicates that the silane modification improved the thermal stability of CHA by limiting thermally induced degradation. This enhanced stability is particularly relevant for biomaterials processing and post-treatment strategies, such as membrane fabrication under irradiation, plasma, or other thermal treatment. In addition, controlled infrared-assisted heating for further functional optimization purposes is possible.

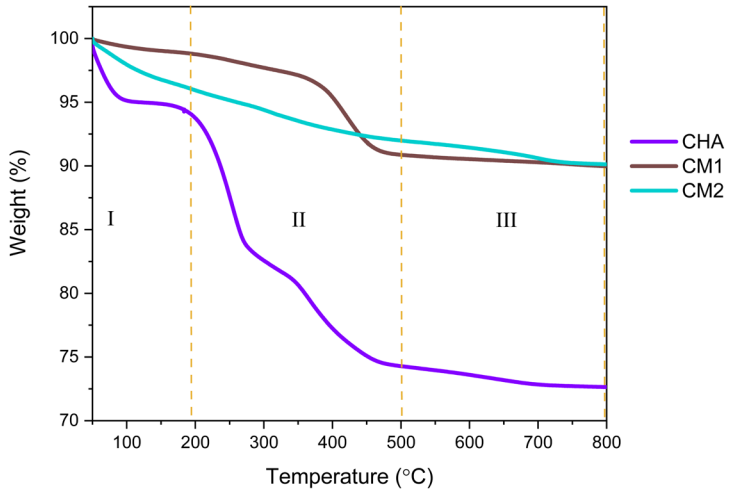

Figure 5. TGA spectra of CHA and silane-modified CHA (variations detailed in Table 1).

4. CONCLUSION

This work presents a systematic evaluation of the influence of silane precursors (TEOS and TMSPMA) and silanization reaction temperature (room temperature and 78.3°C) on the surface modification of CHA. The FTIR analysis showed that the silanol and organosilane groups were grafted on the CHA surface without disrupting the underlying phosphate and hydroxyl chemistry. The XRD spectra confirmed that the apatite structure was preserved after the silanization, with the samples treated at 78.3°C retaining sharper diffraction peaks than those at room temperature. The SEM-EDS results are in agreement with this trend: silicon incorporation was detected only on the modified CHA samples, processed at 78.3°C, with the TEOS-modified CHA (CM1), yielded the highest surface silicon content (0.44%). The TGA thermogram further verified the other characterization results by showing that the silanization at 78.3°C improved thermal stability and reduced the total weight loss from 27.36% (unmodified CHA) to 10.04% (CM1) and 9.88% (CM2).

The results thus demonstrate that in addition to silane type alone, silanization temperature also governs silanization efficiency, with TEOS at 78.3°C (sample CM1) exhibiting the optimal condition among the other studied conditions: maximum silane grafting, preserving crystallinity, and enhancing thermal stability. This study provides a practical window for producing silane-modified CHA as a filler for membranes in regenerative applications, planned for our future work.

AUTHORSHIP CONTRIBUTION STATEMENT

Reza Pahlevi Rudianto: conceptualization, data curation, formal analysis, investigation, methodology, visualization, writing – original draft; Bidhari Pidhatika: funding acquisition, supervision, validation, writing – review & editing; Dida Faadihilah Khrisna: investigation, writing – original draft; Yogi Angga Swasono: validation, writing – review & editing; Syafiqah Saidin: resources, supervision, writing – review & editing.

DATA AVAILABILITY

Data are available within the article or its supplementary materials.

DECLARATION OF COMPETING INTEREST

The authors declare that they have no conflict of interest.

DECLARATION OF GENERATIVE AI

The authors declare that they have not used any type of generative AI for the writing of this manuscript, nor for the creation of graphics, tables, or their corresponding captions. Biorender was used to build Figure 1.

ACKNOWLEDGMENT

This study was supported by Lembaga Pengelola Dana Pendidikan (LPDP) and Badan Riset dan Inovasi Nasional (BRIN) Indonesia through Riset dan Inovasi untuk Indonesia Maju (RIIM) batch 4 with B-3842/II.7.5/FR.06.00/11/2023; B-3855/III.10/FR.06.00/11/2023 grants and through e-Layanan Sains (ELSa).

REFERENCES

(1) Aytaç Z, Dubey N, Daghrery A, Ferreira JA, de Souza Araújo IJ, Castilho M, Malda J, Bottino MC. Innovations in craniofacial bone and periodontal tissue engineering–from electrospinning to converged biofabrication. Int Mater Rev. 2022; 67(4):347–384. https://doi.org/10.1080/09506608.2021.1946236.
(2) Liu Y, Guo L, Li X, Liu S, Du J, Xu J, Hu J, Liu Y. Challenges and tissue engineering strategies of periodontal-guided tissue regeneration. Tissue Eng Part C Methods. 2022; 28(8):405–419. https://doi.org/10.1089/ten.TEC.2022.0106.
(3) Wang X, Chen J, Tian W. Strategies of cell and cell-free therapies for periodontal regeneration: The state of the art. Stem Cell Res Ther. 2022; 13(1):536. https://doi.org/10.1186/s13287-022-03225-z.
(4) Li J, Wang Y, Tang M, Zhang C, Fei Y, Li M, Li M, Gui S, Guo J. New insights into nanotherapeutics for periodontitis: a triple concerto of antimicrobial activity, immunomodulation and periodontium regeneration. J Nanobiotechnology. 2024; 22(1):19. https://doi.org/10.1186/s12951-023-02261-y.
(5) Liu J, Ruan J, Weir MD, Ren K, Schneider A, Wang P, Oates TW, Chang X, Xu HHK. Periodontal bone-ligament-cementum regeneration via scaffolds and stem cells. Cells. 2019; 8(6):537. https://doi.org/10.3390/cells8060537.
(6) Santos MS, Silva JC, Carvalho MS. Hierarchical biomaterial scaffolds for periodontal tissue engineering: recent progress and current challenges. Int J Mol Sci. 2024; 25(16):8562. https://doi.org/10.3390/ijms25168562.
(7) El-Nablaway M, Rashed F, Taher ES, Atia GA, Foda T, Mohammed NA, Abdeen A, Abdo M, Hînda I, Imbrea AM. Bioactive injectable mucoadhesive thermosensitive natural polymeric hydrogels for oral bone and periodontal regeneration. Front Bioeng Biotechnol. 2024; 12:1384326. https://doi.org/10.3389/fbioe.2024.1384326.
(8) Huang TH, Chen JY, Suo WH, Shao WR, Huang CY, Li MT, Li YY, Li YH, Liang EL, Chen YH. Unlocking the future of periodontal regeneration: an interdisciplinary approach to tissue engineering and advanced therapeutics. Biomedicines. 2024; 12(5):1090. https://doi.org/10.3390/biomedicines12051090.
(9) Sun H, Luan J, Dong S. Hydrogels promote periodontal regeneration. Front Bioeng Biotechnol. 2024; 12:1411494. https://doi.org/10.3389/fbioe.2024.1411494.
(10) Yürük G, Demir YD, Vural Ş, Kehr NS. Polymeric biomaterials for periodontal tissue engineering and periodontitis. *RSC Appl Polym*. 2024; 2(4):534–556. https://doi.org/10.1039/D4LP00093E.
(11) Li N, Wang J, Feng G, Liu Y, Shi Y, Wang Y, Chen L. Advances in biomaterials for oral-maxillofacial bone regeneration: spotlight on periodontal and alveolar bone strategies. Regen Biomater. 2024; 11:rbae078. https://doi.org/10.1093/rb/rbae078.
(12) Mysore THM, Patil AY, Hegde C, Sudeept MA, Kumar R, Soudagar MEM, Fattah IMR. Apatite insights: From synthesis to biomedical applications. Eur Polym J. 2024; 209:112842. https://doi.org/10.1016/j.eurpolymj.2024.112842.
(13) Zhao R, Meng X, Pan Z, Li Y, Qian H, Zhu X, Yang X, Zhang X. Advancements in nanohydroxyapatite: synthesis, biomedical applications and composite developments. Regen Biomater. 2025; 12:rbae129. https://doi.org/10.1093/rb/rbae129.
(14) Tran DL, Ta QTH, Tran MH, Nguyen TMH, Le NTT, Nguyen Hong AP, Park HJ, Park KD, Nguyen DH. Optimized synthesis of biphasic calcium phosphate: Enhancing bone regeneration with a tailored β-tricalcium phosphate/hydroxyapatite ratio. Biomater Sci. 2025; 13(4):969–979. https://doi.org/10.1039/d4bm01179a.
(15) Kazimierczak P, Wessely-Szponder J, Palka K, Barylyak A, Zinchenko V, Przekora A. Hydroxyapatite or fluorapatite—which bioceramic is better as a base for the production of bone scaffold?— A comprehensive comparative study. *Int* J Mol Sci. 2023; 24(6):5576. https://doi.org/10.3390/ijms24065576.
(16) Ratnayake J, Gould M, Ramesh N, Mucalo M, Dias GJ. A porous fluoride-substituted bovine-derived hydroxyapatite scaffold constructed for applications in bone tissue regeneration. Materials. 2024; 17(5):1107. https://doi.org/10.3390/ma17051107.
(17) Bystrov VS, Paramonova EV, Avakyan LA, Eremina NV, Makarova SV, Bulina NV. Effect of magnesium substitution on structural features and properties of hydroxyapatite. Materials. 2023; 16(17):5945. https://doi.org/10.3390/ma16175945.
(18) Daghrery A, Bottino MC. Advanced biomaterials for periodontal tissue regeneration. Genesis. 2022; 60(8-9):e23501. https://doi.org/10.1002/dvg.23501.
(19) Imber JC, Imber LC, Roccuzzo A, Stähli A, Muñoz F, Weusmann J, Bosshardt DD, Sculean A. Preclinical evaluation of a new synthetic carbonate apatite bone substitute on periodontal regeneration in intrabony defects. J Periodontal Res. 2024; 59(1):42–52. https://doi.org/10.1111/jre.13203.
(20) Stanislavov AS, Sukhodub LF, Sukhodub LB, Kuznetsov VN, Bychkov KL, Kravchenko MI. Structural features of hydroxyapatite and carbonated apatite formed under the influence of ultrasound and microwave radiation and their

effect on the bioactivity of the nanomaterials. Ultrason Sonochem. 2018; 42:84–96. https://doi.org/10.1016/j.ultsonch.2017.11.011.
(21) Calasans-Maia MD, Melo BR, Alves ATNN, Resende RFB, Louro RS, Sartoretto SC, Granjeiro JM, Alves GG. Cytocompatibility and biocompatibility of nanostructured carbonated hydroxyapatite spheres for bone repair. J Appl Oral Sci. 2015; 23(6):599–608. https://doi.org/10.1590/1678-775720150122.
(22) Priyadharshini SS, Ragavendran C, Sherwood A, Ramya JR, Krithikadatta J. Evaluation of mineral induction ability and cytotoxicity of carbonated hydroxyapatite for pulp tissue regeneration: an in vitro study. Restor Dent Endod. 2024; 49(4):e40. https://doi.org/10.5395/rde.2024.49.e40.
(23) Bian Y, Duan X, Han S, Yuan Y, Shen J, Wang Z, Han B. Application and Research Progress of Carbonated Hydroxyapatite in Bone Tissue Regeneration. Adv Biol. 2026; 10(3): e00451. https://doi.org/10.1002/adbi.202400451.
(24) Turco R, Santagata G, Corrado I, Pezzella C, Di Serio M. In vivo and post-synthesis strategies to enhance the properties of PHB-based materials: A review. Front Bioeng Biotechnol. 2021; 8:619266. https://doi.org/10.3389/fbioe.2020.619266.
(25) Pańtak P, Czechowska JP, Zima A. The influence of silane coupling agents on the properties of α-TCP-based ceramic bone substitutes for orthopaedic applications. RSC Adv. 2023; 13(48):34020–34031. https://doi.org/10.1039/d3ra06027f.
(26) Ghosh R, Gupta S, Mehrotra S, Kumar A. Surface-modified diopside-reinforced PCL biopolymer composites with enhanced interfacial strength and mechanical properties for orthopedic applications. ACS Appl Mater Interfaces. 2024; 16(6):7670–7685. https://doi.org/10.1021/acsami.3c15637.
(27) Oner FK, Alakent B, Soyer-Uzun S. Effect of silane A-174 modifications in the structure, chemistry, and compressive strength of PLA-HAP and PLA-β-TCP biocomposites: Toward the design of polymer–ceramic implants with high performance. ACS Appl Polym Mater. 2021; 3(5):2432–2446. https://doi.org/10.1021/acsapm.1c00054.
(28) Marycz K, Kornicka-Garbowska K, Patej A, Sobierajska P, Kotela A, Turlej E, Kepska M, Bienko A, Wiglusz RJ. Aminopropyltriethoxysilane (APTES)-modified nanohydroxyapatite (nHAp) incorporated with iron oxide (IO) nanoparticles promotes early osteogenesis, reduces inflammation and inhibits osteoclast activity. Materials. 2022; 15(6):2095. https://doi.org/10.3390/ma15062095.
(29) Sugiura Y, Niitsu K, Saito Y, Endo T, Horie M. Inorganic process for wet silica-doping of calcium phosphate. RSC Adv. 2021; 11(20):12330–12335. https://doi.org/10.1039/d1ra00288k.
(30) Rakmae S, Ruksakulpiwat Y, Sutapun W, Suppakarn N. Effect of silane coupling agent treated bovine bone based carbonated hydroxyapatite on in vitro degradation behavior and bioactivity of PLA composites. Mater Sci Eng C. 2012; 32(6):1428–1436. https://doi.org/10.1016/j.msec.2012.04.022.
(31) Liu Q, Matinlinna JP, Chen Z, Ning C, Ni G, Pan H, Darvell BW. Effect of thermal treatment on carbonated hydroxyapatite: Morphology, composition, crystal characteristics and solubility. Ceram Int. 2015; 41(5):6149–6157. https://doi.org/10.1016/j.ceramint.2014.11.062.
(32) Benataya K, Lakrat M, Elansari LL, Mejdoubi E. Synthesis of B-type carbonated hydroxyapatite by a new dissolution-precipitation method. Mater Today Proc. 2020; 31:S83–S88. https://doi.org/10.1016/j.matpr.2020.06.100.
(33) Thool OK, Sasidharan A, Krishna BM, Sabu S, Navaf M, Sunooj KV. Nano-hydroxyapatite (n-HAP) from Pangasius bone side streams and its application as a reinforcing agent in biodegradable food packaging films. Sustain Food Technol. 2025; 3(1):227–238. https://doi.org/10.1039/D4FB00264D.
(34) Syazwan M, Ahmad-Fauzi MN, Balestri W, Reinwald Y, Bi YM. Effectiveness of various sintering aids on the densification and in vitro properties of carbonated hydroxyapatite porous scaffolds produced by foam replication technique. Mater Today Commun. 2021; 27:102395. https://doi.org/10.1016/j.mtcomm.2021.102395.
(35) Rafique MMA. Hydrothermal processing of phase pure and doped hydroxyapatite and its characterization. J Encapsulation Adsorpt Sci. 2018; 8(1):18–37. https://doi.org/10.4236/jeas.2018.81002.
(36) Madupalli H, Pavan B, Tecklenburg MMJ. Carbonate substitution in the mineral component of bone: Discriminating the structural changes, simultaneously imposed by carbonate in A and B sites of apatite. J Solid State Chem. 2017; 255:27–35. https://doi.org/10.1016/j.jssc.2017.07.025.
(37) Jamilludin MA, Dinatha IKH, Supii AI, Partini J, Kusindarta DL, Yusuf Y. Functionalized cellulose nanofibrils in carbonate-substituted hydroxyapatite nanorod-based scaffold from long-spined sea urchin (Diadema setosum) shells reinforced with polyvinyl alcohol for alveolar bone tissue engineering. RSC Adv. 2023; 13(46):32444–32456. https://doi.org/10.1039/d3ra06165e.
(38) Sim YL, Lee J, Oh SM, Kim DB, Kim K, Baeck SH, Shim SE, Qian Y. Mitigation of silicon contamination in fuel cell gasket materials through silica surface treatment. Polymers. 2024; 16(7):914. https://doi.org/10.3390/polym16070914.
(39) Issa AA, Luyt AS. Kinetics of alkoxysilanes and organoalkoxysilanes polymerization: A review. Polymers. 2019; 11(3):537. https://doi.org/10.3390/polym11030537.
(40) Naidu S, Liu C, Scherer GW. Hydroxyapatite-based consolidant and the acceleration of hydrolysis of silicate-based consolidants. J Cult Herit. 2015; 16(1):94–101. https://doi.org/10.1016/j.culher.2014.01.001.
(41) Sugimoto K, Mikami K, Kimura R, Tagaya M. Synthesis of tetraethoxysilane-reacted hydroxyapatite nanoparticles and their stabilization in phosphate-buffered saline. Langmuir. 2023; 39(27):9431–9438. https://doi.org/10.1021/acs.langmuir.3c00954.
(42) John Ł, Janeta M, Rajczakowska M, Ejfler J, Łydżba D, Szafert S. Synthesis and microstructural properties of the scaffold based on a 3-(trimethoxysilyl) propyl methacrylate–POSS hybrid towards potential tissue engineering applications. RSC Adv. 2016; 6(70):66037–66047. https://doi.org/10.1039/C6RA08264E.
(43) Crucho CIC. Synthesis of organoalkoxysilanes: Versatile organic–inorganic building blocks. Compounds. 2023; 3(1):280–297. https://doi.org/10.3390/compounds3010021.

(44) Aneb K, Oudadesse H, Khireddine H, Lefeuvre B, Merdrignac-Conanec O, Tessier F, Lucas A. Study of the effect of ordered porosity and surface silanization on in vitro bioactivity of sol-gel-derived bioactive glasses. Mater Today Commun. 2023; 34:104992. https://doi.org/10.1016/j.mtcomm.2022.104992.
(45) Zhou W, Liu Y, Xiao P, Wang ZW. Dual-layered carbonated hydroxyapatite/polypyrrole: A novel strategy for bone fracture repair implants. J Ind Eng Chem. 2025; 142:225–236. https://doi.org/10.1016/j.jiec.2024.07.027.
(46) Shlykov MA, Putlayev VI, Klimashina ES, Xia Z. Carbonated hydroxyapatite: Mechanisms, properties, and therapeutic applications. Biomater Transl. 2026; 1–17. https://doi.org/10.12336/bmt.25.001758.
(47) Cisneros-Pineda OG, Kao WH, Loría-Bastarrachea MI, Veranes-Pantoja Y, Cauich-Rodríguez JV, Cervantes-Uc JM. Towards optimization of the silanization process of hydroxyapatite for its use in bone cement formulations. Mater Sci Eng C. 2014; 40:157–163. https://doi.org/10.1016/j.msec.2014.03.064.
(48) Karkanis S, Nikolaidis AK, Koulaouzidou EA, Achilias DS. Effect of silica nanoparticles silanized by functional/functional or functional/non-functional silanes on the physicochemical and mechanical properties of dental nanocomposite resins. Appl Sci. 2021; 12(1):159. https://doi.org/10.3390/app12010159
(49) Senra MR, de Lima RB, Souza DH, Marques MV, Monteiro SN. Thermal characterization of hydroxyapatite or carbonated hydroxyapatite hybrid composites with distinguished collagens for bone graft. J Mater Res Technol. 2020; 9(4):7190–7200. https://doi.org/10.1016/j.jmrt.2020.04.089.